

A First-Principles Study of the Nature of the Insulating Gap in VO₂

Christopher S. A. Hendriks

Ambon, Maluku, Indonesia

Master of Science, College of William & Mary, 2013
Bachelor of Arts, Universitas Pelita Harapan, Indonesia, 2007

A Dissertation presented to the Graduate Faculty
of The College of William & Mary in Candidacy for the Degree of
Doctor of Philosophy

Department of Physics

College of William & Mary
August 2020

©2020
Christopher S. A. Hendriks
All rights reserved.

APPROVAL PAGE

This Dissertation is submitted in partial fulfillment of
the requirements for the degree of

Doctor of Philosophy

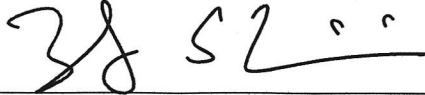


Christopher S. A. Hendriks

Approved by the Committee July 2020


Committee Chair


Henry Krakauer, Professor, Physics
College of William & Mary



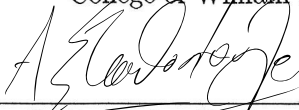
Shiwei Zhang, Professor, Physics
College of William & Mary



Muntaz Qazilbash, Professor, Physics
College of William & Mary



Marc Sher, Professor, Physics
College of William & Mary



Andreas Stathopoulos, Professor, Computer Science
College of William & Mary

ABSTRACT

Upon cooling past a critical temperature $T_c = 340$ K Vanadium dioxide (VO_2) exhibits a metal-insulator transition (MIT) from a metallic rutile R to an insulating monoclinic M1 phase. Other insulating phases, a monoclinic M2 and triclinic T, have been identified and are accessible via strain or doping. Despite decades of research, the nature of the VO_2 MIT is still not fully understood. In this work we present ab-initio hybrid density functional theory (DFT) calculations on the insulating phases, compare the results to experimental measurements and discuss their implications on our understanding of the VO_2 MIT. Recent measurements on M1 VO_2 under high pressure found a transition to a metallic monoclinic state X at $P_c = 34.3$ GPa. Following this increased interest in the study of VO_2 at high pressures, we will also present results of hybrid-DFT calculations on the M1 phase under increasing pressure. Our calculations predict that M1 may become metallic above ~ 32 GPa, in good agreement with experiment.

TABLE OF CONTENTS

Acknowledgments	iii
Dedication	iv
CHAPTER	
1 Introduction	2
2 An Overview of VO ₂	6
2.1 Lattice Structure	8
2.2 Electronic Structure	10
2.2.1 The Band Picture	10
2.2.2 The Role of Strong Electronic Correlation	12
2.3 Density Functional Theory	14
2.3.1 The Problem	14
2.3.2 Mapping the Many-Electron Problem onto a Non-interacting <i>N</i> - electron System	15
2.3.3 Exchange-Correlation Approximations	17
2.3.4 DFT+ <i>U</i>	20
2.3.5 Hybrid Functionals	22
2.4 Overview of Computational VO ₂ Research	23
3 The Insulating Phases of VO ₂ are of Mott-Hubbard Type	26
3.1 Introduction	26
3.2 Experiment	30
3.3 Theory	31

3.4	Results and Discussion	32
3.5	Conclusions	36
4	DFT+ U and HSE Investigation of the VO ₂ Insulator-Metal Transition Under High Pressures	37
4.1	Computational Methods	40
4.2	Results and Discussion	42
4.3	Conclusions	45
5	Conclusions and Outlook	50
	Bibliography	52
	Vita	59

ACKNOWLEDGMENTS

I would like to express my gratitude to my supervisor, Prof. Henry Krakauer for his excellent guidance during my doctoral program. This dissertation would not have been written without his support and understanding throughout my years of research.

I also would like to thank the many members of the Condensed Matter Theory group, past and present, for all the help, discussions and support during my stay in Small Hall.

Finally I would like to thank the William & Mary High-Performance Computing department, especially Eric Walter, for their endless patience and incredible support.

To my parents, without whom I would never have gotten to where I am today.

A FIRST-PRINCIPLES STUDY OF THE NATURE OF THE INSULATING GAP IN
 VO_2

CHAPTER 1

Introduction

Transition metal oxides (TMOs) form one of the most fascinating classes of materials that spans a broad variety of structures and exhibits a diverse array of interesting properties. This versatility and adaptability make them suitable for many scientific and industrial applications, such as microactuators, supercapacitors, and photocatalysts, among many others. Research interest in TMOs are also driven by the complex phenomena they exhibit, which include multiferroicity, superconductivity, long-range magnetic order, and metal-insulator transitions. These arise from the subtle interplay between structural, electronic and magnetic degrees of freedom in these materials, and despite decades of fruitful research there remains much to understand about them.

Of particular interest in this study is the nature of metal-insulator transitions (MITs). In the 1920s the weakly-interacting electronic band picture was developed and used to distinguish between insulators and metals: in the former the highest occupied band was

completely filled, while in the latter it is only partially filled [1–3]. Although initially successful, in 1937 it was reported that contrary to what one would expect from band theory, many TMOs were in fact poor conductors. This led Peierls [4] to note the importance of strong electronic correlation as a possible origin of the insulating behavior, the theory of which was further developed by Mott [5–8].

Unfortunately, many TMOs that exhibit MITs possess large unit cells, complex stoichiometry, require varying degrees of chemical doping or physical strain to induce a transition, or any combination of the above, hindering efforts at understanding the nature of their MITs. So when it was discovered that vanadium dioxide (VO_2) experienced a MIT at 340 K, it was considered an ideal material for study: it had a relatively small unit cell, was stoichiometrically simple, and its near-room-temperature transition point made it practical to experiment on. However, despite its apparent simplicity, the history of research on the material shows us that the nature of its properties are anything but.

As will be discussed in greater detail later, the study of VO_2 spawned a debate on the nature of its MIT that lasted for decades. Briefly, the problem is as follows: due to a partially-filled d -orbital, band theory would lead us to expect VO_2 to be metallic at any temperature. Instead, VO_2 transitions into an insulator at temperatures below 340 K with an energy gap of about 0.6 eV[9]. This electronic transition is accompanied by a structural transition, from a metallic rutile (R) phase to a monoclinic (M1) one. The debate is centered on what exactly causes the emergence of the insulating gap, and researchers are generally split into two camps. Those in favor of the so-called Peierls mechanism argue that

the insulating gap arises as a consequence of the structural changes during the transition. Meanwhile, the opposing group argues that strong electronic correlation is responsible for the insulating gap, and changes to the band structure from structural distortions alone could not be sufficient to explain the observed band gap. A strong argument was made by Pouget *et al.* in 1974 in favor of strong correlation[10], but technical difficulties made experimental verification of this argument impractical at the time.

Meanwhile, foundations were being laid for the practical modeling of physical systems and calculation of their properties. The year 1964 saw the publication of the Hohenberg-Kohn theorems[11], followed in 1965 by the publication of the Kohn-Sham equations[12]. As will be described in further detail in Chapter 2, these works would form the basis of what is now known as density functional theory (DFT). In the decades that followed, refinements to the approximations used in the theory allowed increasingly accurate calculations and models of physical systems. At the same time, the exponential increase of computational power available to researchers made DFT and other computational methods increasingly popular and accessible. Today, DFT has become a workhorse of materials research and is used extensively in the calculation of atomic, molecular, and crystal properties.

This essence of this dissertation is thus the application of DFT to the MIT problem in VO_2 . Therefore this work is organized as follows: Chapter 2 will discuss the debate on the nature of the VO_2 in more detail and lay the theoretical foundation for the rest of the work. Chapter 3 will detail the results of our investigation into the nature of VO_2 , in which we settle the debate over the nature of VO_2 in favor of strong electronic correlation.

In Chapter 4 we investigate the behavior of VO_2 under high pressure and identify two nearly-degenerate phases, one of which transitions into a metallic monoclinic phase under sufficient pressure. Finally, in Chapter 5 we reiterate our conclusions and provide a brief outlook on potential future research.

CHAPTER 2

An Overview of VO₂

The existence of a metal-insulator transition (MIT) in VO₂ was discovered by Morin[9] in 1959. Previously VO₂ was expected to be metallic due to the presence of a partially-filled *d*-orbital, as prescribed by the weakly-interacting electronic band picture. Instead, Morin found that VO₂ exhibited an insulating gap at low temperatures, and transitioned to a metallic state at a critical temperature $T_c \approx 340$ K. In addition, this electronic transition was accompanied by a simultaneous structural phase transition (SPT) from a monoclinic (M1) to a tetragonal rutile (R) crystal structure. Two mechanisms were proposed to explain the insulating phase: strong electronic correlation (Mott-Hubbard) and lattice distortions (Peierls)[13]. However, the concurrent nature of the transition makes it difficult to uncouple the two mechanisms from each other, as the VO₂ M1→R transition exhibits features reminiscent of both.

However, a second monoclinic (M2) and a triclinic (T) state have been identified

and can be stabilized by the application of tensile strain[14] or doping with Cr, Al, or W[10, 15–17], as shown in Fig. 2.1. The presence of these intermediate phases presents a unique opportunity to uncouple the effects of electronic correlation and lattice distortions by avoiding the concurrent MIT and SPT of the M1→R path.

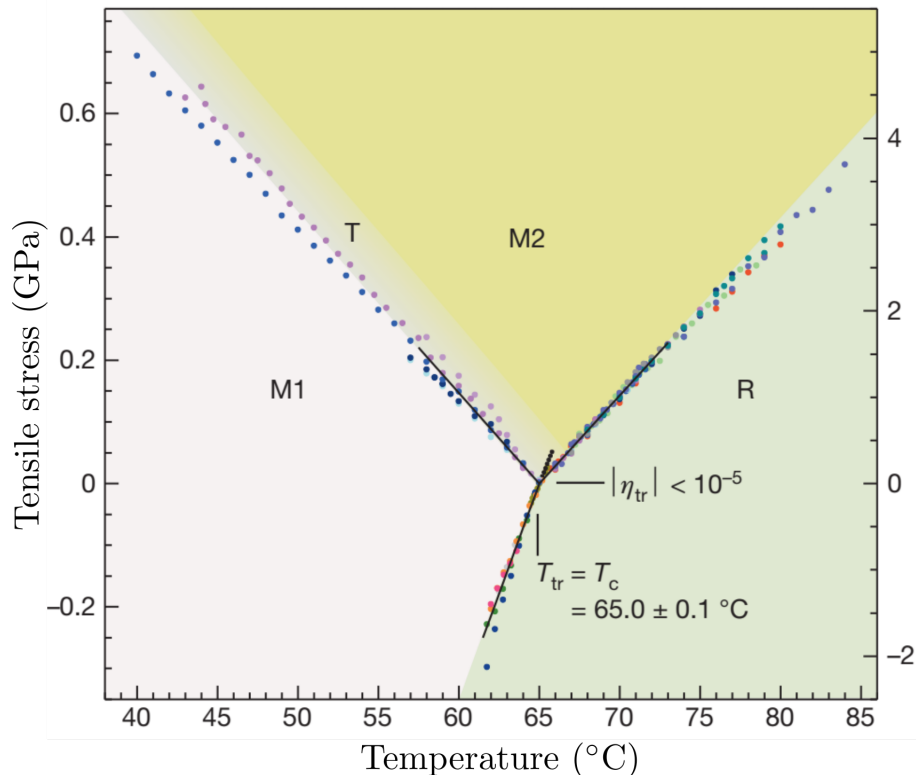


FIG. 2.1: Experimental phase diagram of VO₂ showing the various phases and the triple-point. Adapted from [14].

More recently, experiments conducted on bulk VO₂ under high pressures demonstrate a phase transition from the M1 to a metallic phase X whose structure appears to retain the $P2_1/c$ symmetry of the ground state[18, 19]. Bai *et al.* found that bulk VO₂ in both the M1 and R states undergo a transition to X under sufficiently high pressures. This presents another transition pathway in which the MIT is decoupled from an SPT,

and its investigation may provide further insight into the workings of the VO₂ transition mechanism.

The aim of this chapter is thus to set the stage for the results and discussion on the nature of the insulating gap in VO₂ in the following chapters. The first sections will describe the lattice structure and electronic properties of the known phases of VO₂; this will be followed by a more thorough description of the debate over the mechanism of the insulating gap; the remaining sections will describe the theoretical framework of and touch on the current state of VO₂ research.

2.1 Lattice Structure

Under ambient pressure below T_c , bulk VO₂ takes on a monoclinic M1 structure with space group $P2_1/c$ (#14)[20] and lattice constants $a \approx 5.75 \text{ \AA}$, $b \approx 4.53 \text{ \AA}$, $c \approx 5.38 \text{ \AA}$, $\beta \approx 122.6^\circ$ [21]. Above T_c VO₂ becomes a tetragonal rutile R structure with space group $P4_2/mnm$ (#136) and lattice constants $a = b \approx 4.55 \text{ \AA}$, $c \approx 2.85 \text{ \AA}$ [15]. The second monoclinic structure M2 has been classified as space group $C2/m$ (#12) while the triclinic (T) phase was identified as space group $P\bar{1}$ (#2). The lattice parameters of these insulating phases corresponds approximately to linear combinations of the rutile lattice, and these relationships are shown in Table 2.1.

Setting aside the high-pressure metallic monoclinic phase which has yet to be fully described, there exists a structural relationship between the different lattices that becomes clear upon examination of the positions of the vanadium atoms in each phase. Each

M1	$\mathbf{a}_{M1} \leftrightarrow 2\mathbf{c}_R$	$\mathbf{b}_{M1} \leftrightarrow \mathbf{a}_R$	$\mathbf{c}_{M1} \leftrightarrow \mathbf{b}_R - \mathbf{c}_R$
M2	$\mathbf{a}_{M2} \leftrightarrow 2\mathbf{a}_R$	$\mathbf{b}_{M2} \leftrightarrow 2\mathbf{c}_R$	$\mathbf{c}_{M2} \leftrightarrow -\mathbf{b}_R$
T	$\mathbf{a}_T \leftrightarrow \mathbf{b}_R$	$\mathbf{b}_T \leftrightarrow 2\mathbf{c}_R$	$\mathbf{c}_T \leftrightarrow \mathbf{a}_R$

TABLE 2.1: Approximate relationship between lattice parameters of the insulating phases in terms of the rutile lattice.

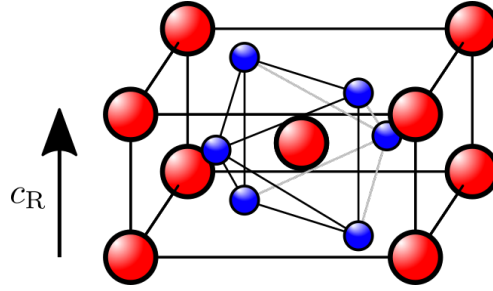


FIG. 2.2: The unit cell of VO_2 in the metallic rutile phase showing the oxygen octahedra surrounding the center vanadium atom. Vanadium and oxygen atom positions are shown as large red and small blue spheres, respectively.

vanadium atom in any one phase belongs to one of two distinct chains oriented along the rutile c_R axis. In the metallic R phase the two chains are equivalent, each forming an equidistant linear array of V atoms along the c_R axis. In the M1 phase the V atoms dimerize and tilt away from the c_R axis equally, so the two chains remain equivalent. This is not the case in the other insulating phases. In M2, half the V atoms dimerize but do not tilt, while the other half form equidistant zig-zag chains along the rutile c_R axis. The triclinic phase can then be understood as an intermediate between the M1 and M2 phases, as vanadium atoms on either chain also dimerize and tilt but to differing degrees such that the chains remain distinct. This is summarized in Fig.2.3.

As will be seen later, this simplified structural framework enables us to more readily consider the effect of the different lattices on their respective electronic structures.

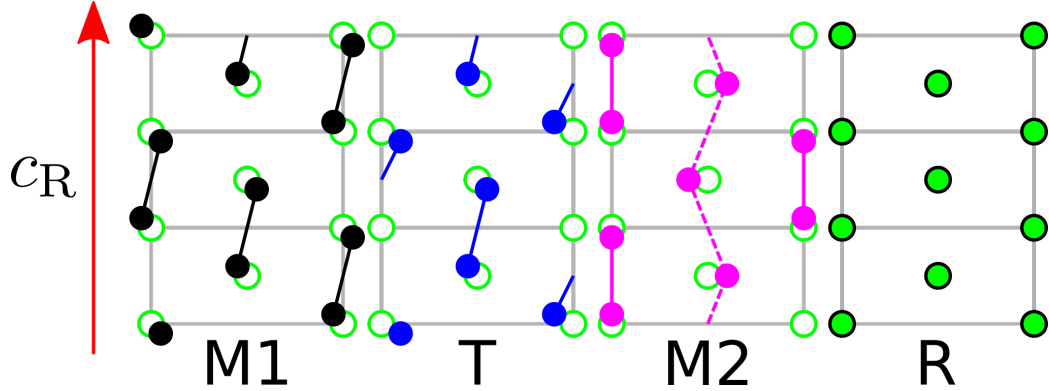


FIG. 2.3: Schematic representation of vanadium atom positions along the rutile c_R in different phases of VO_2 . Solid lines indicate dimerization; dashed lines indicate equidistant atoms. Empty circles and gray lines indicate rutile vanadium positions and rutile unit cells, respectively. Displacements from the rutile positions have been exaggerated for clarity.

2.2 Electronic Structure

2.2.1 The Band Picture

The description of VO_2 and its metal-insulator transition in the weakly-interacting band picture was first analyzed by Goodenough in his foundational 1971 paper [20], and is summarized here. In VO_2 each vanadium atom is surrounded by an oxygen octahedron as shown in Fig. 2.2. We thus have the usual crystal-field splitting of the electronic d -orbitals into upper and lower bands referred to as e_g^σ and t_{2g} , respectively. Now consider the metallic rutile R phase; to further describe the details of the electronic orbitals in this structure, let us define a cartesian coordinate system whose x -axis is directed along the rutile c_R and whose z -axis lies along the line connecting the apical oxygen atoms, as shown in Fig. 2.4. The lobes of the d_{z^2} and d_{xy} orbitals all point toward the negatively-charged oxygen atoms, raising their energies and collectively forming the higher-energy e_g^σ bands. Similarly for the lower-energy t_{2g} bands, the lobes of $d_{x^2-y^2}$ point along the rutile c_R toward

positively-charged vanadium atoms, lowering its energy relative to the other two orbitals. The slight distortion from ideal tetragonal symmetry causes the t_{2g} to split into the a_{1g} ($d_{x^2-y^2}$) and e_g^π (d_{xz} and d_{yz}) bands. With the Fermi level lying within these lower bands, the band picture correctly predicts that the rutile R phase should be metallic.

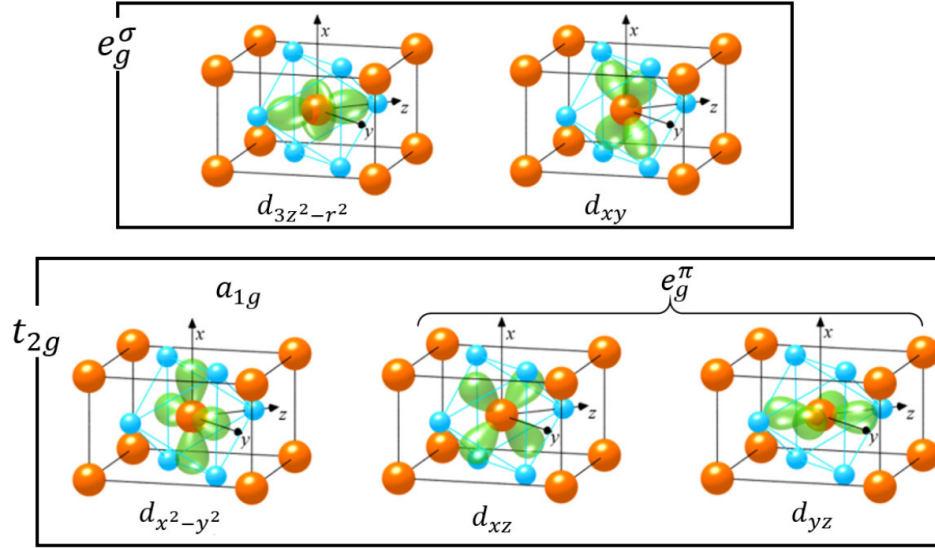


FIG. 2.4: Angular parts of the vanadium d -orbitals within an oxygen octahedron. V atoms are in red, O atoms are in blue. Figure adapted from [22].

In the insulating M1 phase, however, the vanadium atoms dimerize, effectively doubling the unit cell; this splits the a_{1g} band into bonding(a_{1g}) and antibonding(a_{1g}^*) components. Further, the vanadium dimers tilt away from the rutile c_R direction; this increases the energy of the e_g^π bands. These splittings are schematically shown in Fig. 2.5. Thus the main argument of the so-called Peierls mechanism is that together, these two effects fully account for the insulating gap in the monoclinic M1 phase: the dimerization is sufficient to push the bonding a_{1g} band fully below the Fermi level, while the tilt raises the e_g^π well clear of the Fermi level, creating the insulating gap.

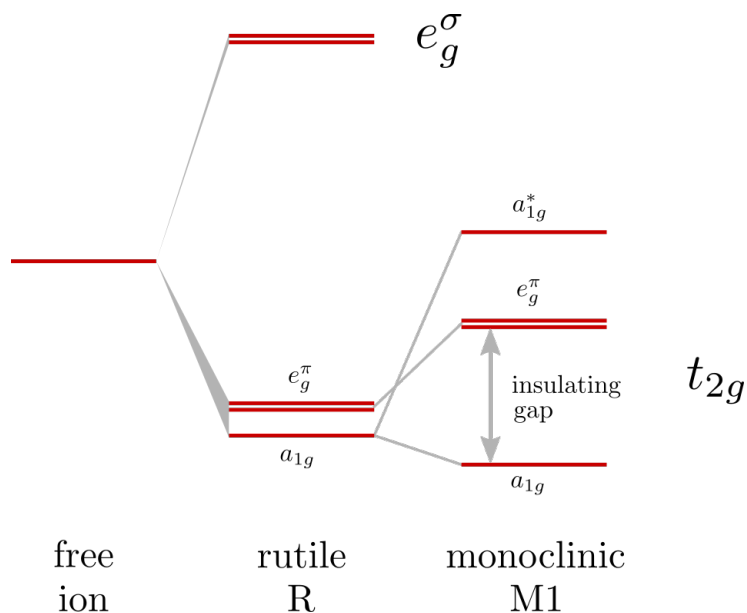


FIG. 2.5: Schematic of d -orbital band splitting in VO_2 .

2.2.2 The Role of Strong Electronic Correlation

The debate on the nature of the MIT in VO_2 is not only a debate on the validity of the band picture, but also one on the role of strong electronic correlation in the opening of the insulating gap. Those in the so-called Peierls camp maintain, as Goodenough did, that the lattice distortions and resulting changes in the electronic bands is sufficient to open an insulating gap during the phase transition. Those in the opposing camp argue that electron-electron many-body correlations are necessary to actually open the insulating gap. Such many-body effects are not captured by standard band structure theory.

Zylbersztein and Mott[23], in particular, have pointed out that the lack of appreciable difference in the size of the band gaps in the three insulating phases, in spite of their structural differences, can only mean that lattice distortions cannot be singularly responsible for the opening of the insulating gap. If they were, then one would expect the M2 phase,

where only half the vanadium chains dimerize, to have either a very small gap or to be metallic in nature. Since this is not the case, they argue that electronic correlation, and not lattice distortion, must be the driving force behind the MIT.

A similar argument was advanced by Pouget *et al.* [10], in which they consider a Hubbard model for a linear chain of dimerized atoms, with U as the intra-atomic Coulomb energy, t the intra-dimer hopping matrix element, and t' the inter-dimer hopping integral. This one-dimensional chain is analogous to the chain of vanadium atoms along the rutile c_R direction in VO_2 . In the band limit where $t \gg U$ the insulating gap would be $E \approx 2|t - t'|$, while in the localized limit of $t \ll U$ the gap would be $E \approx U - 2|t'|$. In the M1 phase, where all vanadium atoms form equivalent dimers, it would be difficult to distinguish between the two limiting cases. However, Pouget *et al.* pointed out that a clear distinction can be made when $t \rightarrow t'$, which is the case for the linear chains in the M2 phase. Moreover, their NMR measurements show the presence of localized $3d$ electrons in the equidistant vanadium chains of the M2 phase, implying $t \ll U$ for that phase.

Despite the strength of this argument, technical difficulties and lack of computational power in the past has prevented its confirmation until very recently. In Chapter 3 we will present the first experimental measurements and theoretical calculations of the optical conductivities of VO_2 in the insulating phases (M1, M2, T) in confirmation of this argument for the role of correlation in the MIT in VO_2 .

2.3 Density Functional Theory

2.3.1 The Problem

In quantum mechanics, the energies and evolution of a system are fully described by the Schrödinger equation

$$\hat{H}\psi_i = E_i\psi_i \quad (2.1)$$

where \hat{H} is the Hamiltonian of the system, E_i are its energies and ψ_i its wavefunctions. For a system consisting of multiple nuclei and electrons, we can express the Hamiltonian in atomic units (where $\hbar = 1$, $m_e = 1$, and $e = 1$) as

$$\hat{H} = -\frac{1}{2} \sum_{i=1}^{N_e} \nabla_i^2 - \frac{1}{2} \sum_{\alpha=1}^N \frac{1}{M_\alpha} \nabla_\alpha^2 - \sum_{i=1}^{N_e} \sum_{\alpha=1}^N \frac{Z_\alpha}{r_{i\alpha}} + \sum_{i=1}^{N_e} \sum_{j>i}^{N_e} \frac{1}{r_{ij}} + \sum_{\alpha=1}^N \sum_{\beta=1}^N \frac{Z_\alpha Z_\beta}{r_{\alpha\beta}} \quad (2.2)$$

where N and N_e are the total number of nuclei and electrons, respectively; latin indices denote electrons while greek indices denote nuclei. This Hamiltonian can be further simplified using the Born-Oppenheimer approximation ($M_\alpha \gg 1$), eliminating the nuclear kinetic term. Dropping the constant ion-ion coulomb term, we are left with

$$\hat{H} = -\frac{1}{2} \sum_{i=1}^{N_e} \nabla_i^2 + \sum_{i=1}^{N_e} \sum_{j=1}^{N_e} \frac{1}{r_{ij}} + V_{\text{ext}}$$

The problem is now reduced to solving the Schrödinger equation for an interacting system of electrons in an external potential V_{ext} . This external potential includes the electron-ion term and any external electric and magnetic fields. That said, solving this electronic-

only Schrödinger equation is an intractable problem for systems with a large number of electrons.

2.3.2 Mapping the Many-Electron Problem onto a Non-interacting N -electron System

Density Functional Theory (DFT) provides a framework to solve this problem for realistic systems. It starts with the Hohenberg-Kohn (HK) theorems, which state that

1. the ground state energy of a system of electrons is a unique *functional* of the ground state electron density ($E_{\text{GS}} = E[n_{\text{GS}}]$), and that
2. this ground state energy can be obtained via the variational principle – that is, the electron density that minimizes the total energy of the system is in fact the ground state electron density.

Proof of these theorems are relatively straightforward and have been covered extensively elsewhere so they will not be repeated here[11]. These theorems form the basis of the Kohn-Sham formulation of DFT[12], where the many-body interacting electron system is mapped into a *fictitious* system of noninteracting electrons within an effective potential that nevertheless yields the same ground state density and energy as the original system.

In their formulation Kohn and Sham expressed the total energy functional of this

fictitious system as

$$E[n] = T_{\text{KS}}[n] + E_{\text{H}}[n] + E_{\text{XC}}[n] + \int v_{\text{ext}}(\mathbf{r}) n(\mathbf{r}) d\mathbf{r} \quad (2.3)$$

where

$$T_{\text{KS}} = \sum_{i=1}^N \int \phi_i^*(\mathbf{r}) \left(-\frac{1}{2} \nabla^2 \right) \phi_i(\mathbf{r}) d\mathbf{r} \quad (2.4)$$

is the non-interacting Kohn-Sham kinetic energy,

$$E_{\text{H}} = \int \frac{n(\mathbf{r}) n(\mathbf{r}')}{|\mathbf{r} - \mathbf{r}'|} d\mathbf{r} d\mathbf{r}' \quad (2.5)$$

is the classical Hartree (Coulomb) interaction energy, and E_{XC} is the so-called *exchange-correlation* energy, a catch-all term that includes contributions to the total energy not covered by the other terms. This includes but is not limited to the self-energy correction to the Hartree term, electron-electron interaction energies, and corrections to the kinetic term due to said interaction effects.

Expressing the density of the fictitious system as $n(\mathbf{r}) = \sum_i^N \phi_i^* \phi_i$, minimizing the energy yields the Euler-Lagrange equations for the ϕ_i

$$\left(-\frac{1}{2} \nabla^2 + v_{\text{eff}}(\mathbf{r}) \right) \phi_i(\mathbf{r}) = \varepsilon_i \phi_i(\mathbf{r})$$

an effectively one-particle Schrödinger equation, with ε_i being the energy of the Kohn-

Sham orbital ϕ_i .

The Hohenberg-Kohn theorems say E_{XC} exists, but unfortunately its exact expression is unknown. In implementing the Kohn-Sham procedure, one must choose an approximate form for this functional. This will be discussed in more detail in the next section. Thus the Kohn-Sham effective potential can be calculated from the density as

$$v_{\text{eff}}(\mathbf{r}) = \int \frac{n(\mathbf{r}')}{|\mathbf{r} - \mathbf{r}'|} d\mathbf{r}' + \frac{\delta E_{\text{XC}}[n]}{\delta n(\mathbf{r})} + v_{\text{ext}}(\mathbf{r}) \quad (2.6)$$

Solving for the ground state density thus becomes a self-consistent iterative process:

1. Begin with an initial guess to the ground state density.
2. Use this density to construct the effective potential v_{eff} .
3. Solve the Schrödinger-like equation to obtain the Kohn-Sham orbitals ϕ_i , and calculate the total energy.
4. Construct a new ground state density from the calculated orbitals.
5. Repeat steps 2-4 until new density and total energy do not change appreciably.

2.3.3 Exchange-Correlation Approximations

The exchange-correlation functional E_{XC} and resulting potential v_{XC} are the only truly unknown quantities in the Kohn-Sham formulation of DFT; thus in principle if we knew the exact form of the exchange-correlation functional for a given system then we could

determine its exact ground state density and calculate its properties.

Luckily, it turns out that even approximate forms of the exchange-correlation functional can yield useful predictions of physical properties of many real systems and materials. We will now briefly mention a few forms that are particularly relevant to the research presented in this dissertation.

Local Density Approximation (LDA)

The *Local Density Approximation* is one of the simplest approximations of the exchange-correlation functional, and is based on the assumption that the term depends only on the density at the point where the functional is being evaluated,

$$E_{\text{XC}}^{\text{LDA}}[n] = \int \varepsilon_{\text{XC}}^{\text{LDA}}(n) n(\mathbf{r}) d^3\mathbf{r} \quad (2.7)$$

with ε_{XC} being the exchange-correlation energy per electron of a *homogeneous electron gas* of density $n(\mathbf{r})$. In this formulation, the exchange-correlation energy is split into its exchange and correlation components,

$$E_{\text{XC}}^{\text{LDA}} = E_{\text{X}} + E_{\text{C}} \quad (2.8)$$

$$= -\frac{3}{4} \left(\frac{3}{\pi}\right)^{\frac{1}{3}} \int \{n(\mathbf{r})\}^{\frac{4}{3}} d\mathbf{r} + E_{\text{C}} \quad (2.9)$$

where the exchange term is that of the homogeneous electron gas. No exact expression exists for the correlation term; approximations exist for the edge cases of very weak and

very strong correlation, and numerical quantum Monte Carlo simulations have been performed for certain intermediate cases. Different approaches and approximations to the correlation term have thus given rise to various "flavors" of LDA, such as the Vosko-Wilk-Nusair (VWN), Perdew-Zunger (PZ81), and Perdew-Wang (PW92) functionals. Despite its relative simplicity, the LDA has been successfully used to calculate various properties of solids.

Generalized Gradient Approximation (GGA) and Beyond

The logical extension of the LDA would be to incorporate local gradient effects; thus the *Generalized Gradient Approximation* defines the exchange-correlation functional as

$$E_{\text{XC}}^{\text{GGA}}[n] = \int \varepsilon_{\text{XC}}^{\text{GGA}}(n, \nabla n) n(\mathbf{r}) d^3\mathbf{r} \quad (2.10)$$

As in the case of LDA, there exists many different flavors of GGA functionals, both empirical and non-empirical. While empirical GGA functionals are often fitted to certain sets of molecules or materials and thus perform well only for those systems, non-empirical functionals are usually fitted to more general physical constraints and are generally applicable to more systems. Examples of the latter include the Perdew-Burke-Ernzerhof (PBE), Perdew-Wang (PW91), and the Armiento-Mattsson (AM05) functionals.

From here the natural progression would be to include the second derivative of the density in the approximation to the exchange-correlation functional. This class of functionals are collectively known as *meta-GGA* functionals, and show improvements over GGA

functionals in the calculation of certain physical properties. The Tao-Perdew-Staroverov-Scuseria (TPSS) functional is an example of a meta-GGA functional.

2.3.4 DFT+ U

Despite its widespread success in describing the properties of many different materials and systems, DFT often fails to properly describe systems with localized (and hence strongly correlated) electrons. One attempt to correct this issue is to introduce a strong intra-atomic interaction in a screened Hartree-Fock-like manner, which is commonly referred to as the DFT+ U approach[24, 25].

The two most popular implementations of this approach are those introduced by Liechtenstein *et al.*[24] and Dudarev *et al.*[25]. In general both depend on two parameters: the Hubbard-like onsite repulsion term U and the onsite exchange term J , though in the Dudarev approach only an "effective" $U_{\text{eff}} = U - J$ is relevant. The specific implementation of these methods vary, but in general they involve additional (somewhat ad-hoc) term(s) to the DFT total energy. Since this work utilizes the Vienna Ab-initio Software Package (VASP) throughout, we will briefly describe its specific implementation. The Liechtenstein method writes the total energy as

$$E_{\text{DFT}+U} = E_{\text{DFT}} + E_{\text{HF}} - E_{\text{DC}} \quad (2.11)$$

where E_{HF} is the Hartree-Fock-like term, and E_{DC} is the double counting energy. The

former is of the form

$$E_{\text{HF}} = \frac{1}{2} \sum_{\{\gamma\}} (U_{\gamma_1\gamma_3\gamma_2\gamma_4} - U_{\gamma_1\gamma_3\gamma_4\gamma_2}) \hat{n}_{\gamma_1\gamma_2} \hat{n}_{\gamma_3\gamma_4}$$

with $\hat{n}_{\gamma_1\gamma_2}$ being the on-site occupancies

$$\hat{n}_{\gamma_1\gamma_2} = \langle \phi^{s_2} | m_2 \rangle \langle m_1 | \phi^{s_1} \rangle$$

and $U_{\gamma_1\gamma_3\gamma_2\gamma_4}$ being the on-site electron-electron interaction

$$U_{\gamma_1\gamma_3\gamma_2\gamma_4} = \langle m_1 m_3 | \frac{1}{|\mathbf{r} - \mathbf{r}'|} | m_2 m_4 \rangle \delta_{s_1 s_2} \delta_{s_3 s_4}$$

Meanwhile, the double counting term takes the form

$$E_{\text{DC}} = \frac{U}{2} n_{\text{tot}} (n_{\text{tot}} - 1) - \frac{J}{2} \sum_{\sigma} n^{\sigma} (n^{\sigma} - 1) \quad (2.12)$$

with $n_{\text{tot}} = \sum_{\sigma} n^{\sigma}$. The Dudarev approach is simpler and modifies the DFT total energy as follows:

$$E_{\text{DFT}+U} = E_{\text{DFT}} + \frac{(U - J)}{2} \sum_{\sigma} \left[\left(\sum_{m_1} n_{m_1, m_1}^{\sigma} \right) - \left(\sum_{m_1, m_2} n_{m_1, m_2}^{\sigma} n_{m_2, m_1}^{\sigma} \right) \right] \quad (2.13)$$

with the occupancy matrix elements as defined above. The appropriate values of U (and J) vary by system and are often obtained by fitting the calculation results to known

experimental quantities. Further details on the implementation can be found in Refs.[24–27]

2.3.5 Hybrid Functionals

Aside from the preceding exchange-correlation functionals, there exist a class of functionals that incorporate a portion of exact *Hartree-Fock exchange* along with the usual empirical or non-empirical exchange-correlation terms. These functionals are called *hybrid functionals*, and the exact Hartree-Fock(HF) exchange term they incorporate can be expressed as

$$E_X^{\text{HF}} = -\frac{1}{2} \sum_{i,j} \int \phi_i^*(\mathbf{r}_1) \phi_j^*(\mathbf{r}_2) \frac{1}{r_{12}} \phi_j(\mathbf{r}_1) \phi_i(\mathbf{r}_2) d\mathbf{r}_1 d\mathbf{r}_2 \quad (2.14)$$

Thus a hybrid functional will consist of a linear combination of E_X^{HF} and any number of other exchange and/or correlation density functionals. For example, the PBE0 hybrid functional is expressed as

$$E_{\text{XC}}^{\text{PBE0}} = \frac{1}{4} E_X^{\text{HF}} + \frac{3}{4} E_X^{\text{PBE}} + E_C^{\text{PBE}} \quad (2.15)$$

As the results presented in chapters 3 and 4 were obtained using the Heyd-Scuseria-Ernzerhof (HSE) hybrid functional, it would be appropriate to discuss it in more detail here. In addition to incorporating a fraction of exact HF exchange, the HSE functional also separates its exchange terms into so-called short-range and long-range components;

thus it is also sometimes referred to as a range-separated hybrid functional. Specifically, the HSE functional is expressed as

$$E_{\text{XC}}^{\text{HSE}} = \alpha E_{\text{X}}^{\text{HSE,SR}}(\mu) + (1 - \alpha) E_{\text{X}}^{\text{PBE,SR}}(\mu) + E_{\text{X}}^{\text{PBE,LR}}(\mu) + E_{\text{C}}^{\text{PBE}} \quad (2.16)$$

The superscripts SR and LR refer to short-range and long-range components, respectively; the *mixing parameter* α denotes the fraction of exact HF exchange; finally, μ is a parameter that controls the range separation. The creators of the functional originally set $\alpha = 0.25$ as in PBE0, and found the optimal value for the range parameter to be $\mu = 0.3 \text{ \AA}^{-1}$; these choices of parameters yield what is now known as the HSE03 functional. They later revised their range parameter to $\mu = 0.2 \text{ \AA}^{-1}$ while keeping $\alpha = 0.25$, yielding what is now referred to as the HSE06 functional.

Although HSE03 and HSE06 are the most commonly used variants of HSE, it has been shown that treating α as an material-dependent parameter can yield computed parameters that are in better agreement with experimental values[28, 29]. Moreover, it has also been shown that α can be semi-quantitatively related to the Hubbard U in DFT+ U [30]. This is the approach that is adopted in this work.

2.4 Overview of Computational VO₂ Research

If we accept that VO₂ is a strongly-correlated material, then it is not terribly surprising that early DFT calculations on VO₂ yielded unphysical results. LDA calculations

performed by Wentzcovitch *et al.* found the M1 phase to be a semimetal with an energy gap ≈ 0.04 eV, whereas experiment firmly classifies M1 as an insulator with a band gap of about 0.6 eV [31, 32]. A similar LDA treatment of the M1 and M2 insulating phases by Eyert [22] also failed to open an insulating gap. Later calculations by Eyert using GGA [33] similarly found a metallic ground state, underscoring the inadequacy of standard DFT in describing the insulating phases of VO₂.

Later work by Huffman *et al.* reported DFT+ U calculations on the M1 phase with a value of $U \geq 3$ eV that does open up an insulating gap and yields phonon frequencies that are in good agreement with measured values [34]. We found similar results in our own DFT+ U calculations. As will be discussed in the next chapter, we also note certain features at or around the band gap energy in the calculated M1 and M2 optical conductivities that are inconsistent with experimental measurements, and find that DFT+ U shares the same problem as regular DFT of incorrectly predicting the antiferromagnetic M2 as the lowest-energy phase.

In his 2011 Letter Eyert also reported hybrid-DFT calculations on VO₂ using one of the standard HSE functionals [33]. Although correct in identifying the antiferromagnetic ordering as the lowest energy state of the M2 phase, his HSE calculations also yielded insulating gaps of about 1.1 eV in the M1 phase and about 1.2 eV in the M2, an overestimation of the experimental gaps by roughly a factor of two.

A number of studies have also been performed using Dynamical Mean-Field Theory (DMFT), with varying results and conclusions. Initial calculations by Biermann *et*

al. employing the usual single-site impurity model on the vanadium atoms in M1 fail to open an insulating gap[35], making it clear that a cluster-DMFT (cDMFT) approach with both V atoms in the dimer pair as impurity sites would be necessary. Describing M1 as a "correlation-assisted Peierls insulator," Biermann *et al.* argue that while correlation is necessary to open the insulating gap, the material remains Peierls-like since its energy bands do not exhibit the usual features of Mott-Hubbard insulators[36]. Conversely, Kotliar *et al.* describe the R→M1 MIT as a "Peierls-assisted orbital selective Mott transition" and a "Mott transition in the presence of strong intersite exchange"[37, 38]. The calculated electronic structures for the M1 and M2 phases reported in Ref. [38] are quite similar to each other, in line with the arguments set forth by Mott and others [10, 23].

Finally, in recent years there has been increasing interest in VO₂ under high pressures. Following experimental reports of metallization of monoclinic VO₂ under sufficiently high pressures [18, 19], He *et al.* performed DFT+*U* calculations on the insulating M1 phase under increasing pressures [39]. Their calculations identified two structurally similar phases that were nearly degenerate, which they labeled M1' and M1". These phases are mainly differentiated by opposite rotations of their oxygen octahedra about the rutile *c*-axis with respect to the ambient-pressure M1 structure. Interestingly, the behavior of these phases under increasing pressure differed greatly: while M1' would maintain an insulating gap, M1" would become metallic at 40 GPa. The authors therefore suggested M1" as a possible explanation for the observed metallization of monoclinic VO₂. This will be discussed further in Chapter 4.

CHAPTER 3

The Insulating Phases of VO_2 are of Mott-Hubbard Type

3.1 Introduction

Numerous experimental and theoretical studies of the metal-insulator transition (MIT) between the insulating monoclinic M1 and the metallic rutile R phases of vanadium dioxide (VO_2) have been performed since its identification by Morin in 1959. While some attribute the opening of the insulating gap to the dimerization of the vanadium atoms (so-called Peierls-type mechanism) in the M1 phase, others argue that although the dimerization plays a role, the primary driving force behind the MIT is in fact Mott-Hubbard electronic correlation. These studies have been the subject of extensive reviews[13, 40, 41] and will therefore not be referenced directly here. A significant proportion of the literature on

the nature of insulating VO₂, particularly in recent years [36, 37, 42–53], has struggled to decouple the contributions of the Mott-Hubbard and Peierls mechanisms because of an emphasis on the M1 phase. Interestingly, it has long been recognized that measuring the electronic properties of two additional insulating VO₂ phases, the monoclinic M2 and triclinic T, could potentially settle the debate about the origin of the energy gap, but the measurements have been difficult to achieve.

One of our purposes in this chapter is to refocus attention to the importance of measuring the electronic properties of the monoclinic M2 and triclinic (T) phases to decouple the effects of the Peierls and Mott-Hubbard mechanisms. This can be seen from the argument put forward by Pouget et al.[10], which can be summarized as follows: One starts from a model of an isolated vanadium dimer in VO₂, with one electron per site, analogous to the familiar case of the hydrogen molecule. Both the Peierls and Mott-Hubbard pictures correspond to limiting cases of the Hubbard model for a chain of such dimers, depending on whether the intradimer hopping parameter (t) or the intra-atomic Coulomb repulsion (U), respectively, is the dominant energy scale in the system. Interestingly, in both cases, the qualitative description of the electronic structure is the same: an insulator with a bonded spin singlet on the dimer, where the band gap results from splitting of the bonding and antibonding a_{1g} bands (the lower and upper Hubbard bands in the Mott picture). As pointed out by the authors of Ref.[10], the only clear distinction between the two cases is how the energy gap responds to changes in the hopping parameter resulting from changes in lattice structure. For the chain of dimers, the bands broaden relative to

the isolated dimer, decreasing the gap based on the interdimer hopping (t'). In the Peierls limit ($U \ll t, t'$), insulating behavior vanishes as t approaches t' , the case of undimerized chains. In contrast, the gap is primarily set by U in the Mott-Hubbard limit ($U \gg t, t'$), and is thus insensitive to changes in the degree of dimerization. In the M1 phase, where all of the chains are dimerized and equivalent, it is difficult to decouple the effect of dimerization from intraatomic Coulomb correlations. This is not the case for the M2 and T phases.

In this chapter, we present the result of hybrid-functional calculations on the electronic structure of VO_2 . These calculations go beyond the Hubbard model for a chain of vanadium dimers and take into account the multiband nature of the electronic structure. The calculations were motivated by our experimental collaborators, the Qazilbash group at the College of William & Mary, who performed infrared microspectroscopy and spectroscopic microellipsometry on internally strained VO_2 crystals that undergo a first order phase transition with increasing temperature from the T phase to the M2 phase. Both our calculations and the experimental measurement find that the energy gap and electronic structure are essentially unchanged across this structural phase transition. Moreover, the optical energy gap of 0.6 (± 0.1) eV in the M2 and T phases is nearly the same as that measured by numerous previous measurements on the M1 phase[46, 54–58]; the gap is insensitive to the different vanadium pairing arrangements in the M1, M2, and T phases. This indicates that the gap has a common physical origin in the intra-atomic Coulomb correlations in the insulating phases of VO_2 .

In the M1 phase, all of the vanadium ions dimerize and tilt in equivalent chains along the rutile c_R axis (see Fig. 1). In contrast, the M2 phase contains two distinct types of vanadium chains: one type consists of vanadium ions that pair but do not tilt, while the other consists of vanadium ions that tilt but do not pair. The vanadium ions in the latter chain are equidistant, each carrying a localized electron with a spin-1/2 magnetic moment and antiferromagnetic exchange coupling between nearest neighbors[10, 59]. The T phase has two types of inequivalent vanadium chains (or sublattices) in which the vanadium ions are paired and tilted to different degrees (see Fig. 1)[10]. The T phase can be thought of as an intermediate phase between the M2 and M1 phases, where the chains become equivalent in M1. While the M1 insulating phase is generally found in bulk VO_2 , the M2 and T phases can be accessed via chemical doping or strain[10, 60–66].

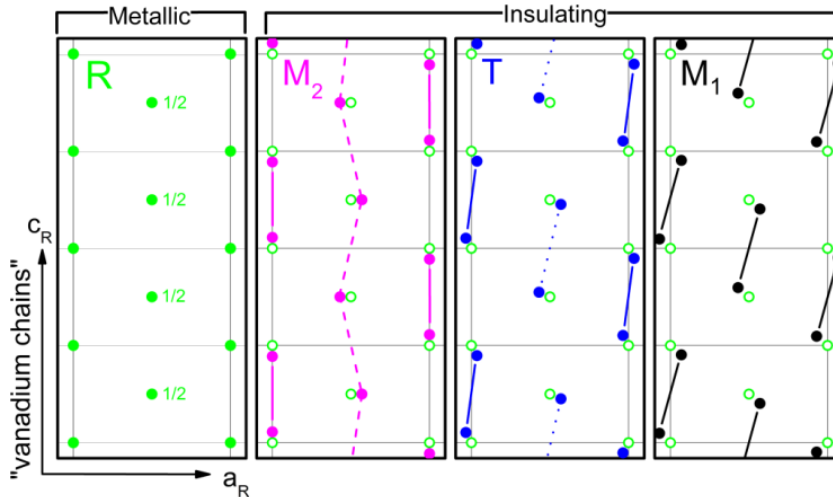


FIG. 3.1: A plan view of vanadium ion positions for the metallic rutile and insulating M2, T, and M1 phases of VO_2 . In all phases, the vanadium ions at the center of each rutile unit cell (shown by the grid lines) are offset from the others by $\frac{1}{2}$ unit cell (denoted by "1/2" in the rutile panel). The vanadium ions in the insulating phases undergo small displacements from the rutile positions (open green circles in the panels of the insulating phases). The rutile lattice vectors c_R and a_R are shown in the lower left corner of the diagram. Vanadium chains in the insulating phases are oriented along the c_R direction.

Nuclear magnetic resonance (NMR) and electron paramagnetic resonance (EPR) have determined the presence of localized d electrons with about one Bohr magneton magnetic moment on the unpaired vanadium chains of the M2 phase[10, 62, 63]. While this localization is a hallmark of a Mott-Hubbard insulator, the situation in the dimerized chains is less clear. The NMR and EPR measurements can be interpreted using a model in which the electrons on the dimerized chains are covalently bonded. Therefore, as alluded to above, it is unclear whether the dimerized chains should be thought of as Peierls insulators, or Mott-Hubbard insulators with the valence electrons forming covalently bonded singlets which are localized on the dimers. It has been argued that the M1 and T insulating phases of VO₂, which differ only slightly in free energy from the M2 phase, cannot have a grossly different energy gap and should thus also be classified as Mott-Hubbard insulators[10, 32]. Although strong, this argument needs experimental verification via direct measurement of the M2 and T phase energy gaps, which can then be compared to each other and to the literature values of the M1 phase energy gap.

3.2 Experiment

The samples used in measurements by our collaborators are rod-shaped single crystals with lengths and widths varying between 1 – 3 mm and 50 – 100 μ m, respectively. These single crystal samples are oriented such that the rutile c_R direction in each sample lies parallel to the long axis of the crystal. These single crystals allow for measurements of anisotropic properties using infrared spectroscopy and spectroscopic microellipsometry

across the R→T→M2 transitions on the *same* sample, minimizing potential issues that can stem from collecting and comparing measurements from different samples. Raman spectroscopy and observation of changes in sample sizes further confirm the phase assignments of the samples used in measurements.

Generalized spectroscopic microellipsometry between 0.6 and 5.5 eV (~ 4800 and $\sim 44000 \text{ cm}^{-1}$) was performed at William & Mary. Spectroscopic ellipsometry allows accurate determination of both real and imaginary parts of the optical constants of the sample, which in turn allows investigation of the material's electronic structure.

3.3 Theory

We then performed ab initio hybrid density functional theory (DFT) calculations on the three insulating phases with the Heyd-Scuseria-Ernzerhof (HSE) functional [67, 68]. The imaginary part of the frequency-dependent dielectric tensor was obtained from DFT wavefunctions[69],

$$\epsilon_{\alpha\beta}^{(2)}(\omega) = \frac{4\pi^2 e^2}{\Omega} \lim_{q \rightarrow 0} \frac{1}{q^2} \sum_{c,v,\mathbf{k}} 2w_{\mathbf{k}} \delta(\epsilon_{c\mathbf{k}} - \epsilon_{v\mathbf{k}} - \omega) \times \langle u_{c\mathbf{k}+\mathbf{e}_{\alpha q}} | u_{v\mathbf{k}} \rangle \langle u_{v\mathbf{k}} | u_{c\mathbf{k}+\mathbf{e}_{\beta q}} \rangle$$

where the indices c and v refer to conduction and valence states, respectively, $w_{\mathbf{k}}$ are k-point weights, and $u_{c\mathbf{k}}$ is the periodic part of the orbital wavefunctions at \mathbf{k} . The real part

can then be obtained from a Kramers-Kronig transformation,

$$\epsilon_{\alpha\beta}^{(1)}(\omega) = 1 + \frac{2}{\pi} P \int_0^{\infty} \frac{\epsilon_{\alpha\beta}^{(2)}(\chi) \chi}{\chi^2 - \omega^2 + i\eta} d\chi$$

Calculated optical conductivities were determined from the imaginary part of the optical dielectric tensor, using the Vienna Ab initio Simulation Package (VASP) [70–73] with HSE (screened) exact-exchange fraction $\alpha = 0.05$ and screening parameter $\mu = 0.2$. The optical conductivity calculations are for vertical-only transitions (initial and final states are at the same k-point). The theoretical conductivities were broadened by 0.3 eV, except as indicated, to account for quasiparticle lifetime effects not included in HSE. With suitably chosen α , the HSE functional can, in many instances, provide a good description of electronic properties ranging from band to Mott-Hubbard insulators as shown in previous work [28, 29]. The percentage α of exact exchange in hybrid DFT can be semiquantitatively related to the value of the Hubbard U parameter in DFT+ U , with larger values of α (and U) yielding larger optical gaps [28–30]. Hybrid DFT and DFT+ U both provide a mean-field treatment of on-site $3d$ correlation on the V atoms. Previous M1 and M2 HSE calculations [33, 74] used $\alpha = 0.25$ calculations, which yielded too large band gaps, compared to experiment¹.

¹Eyert’s 2011 Letter (Ref. [33]) references both HSE papers, Refs [67] and [68]. While not made explicit, we assume Eyert used the more common HSE06 from Ref. [68]. In either case, both HSE03 and HSE06 sets $\alpha = 0.25$.

3.4 Results and Discussion

Optical conductivities reported by our experimental collaborators are shown in Fig.3.2(a)-(b). It is immediately clear that the optical conductivity, and thus the electronic structure, of the M2 and T phases is nearly the same. This finding is remarkable given that there are obvious differences in the structural and magnetic properties between the two phases, as discussed above. Interestingly, numerous measurements on single crystals and thin films of the M1 phase give almost the same magnitude of the energy gap as measured in the M2 and T phases [46, 54–58]. The optical energy gap is the spectral region with vanishing conductivity. Above the gap, the optical interband transition labeled Δ , is quite rigid across this wide range of VO₂ samples.

For a direct comparison to the M1 phase, Fig.3.2(a)-(b) also shows optical conductivity extracted from the reflectance spectrum of Verleur *et al.* on single crystals [75]. The complex conductivity is not uniquely determined by the reflectance intensity spectrum without knowledge of the reflectance phase. In addition to the optical conductivity reported in Ref. [75], our collaborators presented an alternative determination of the optical conductivity using the T phase complex conductivity measured here to approximate the value of the M1 reflectance phase shift in the high-energy region of the spectrum. Using this constraint leads to an M1 conductivity spectrum with a lower uncertainty than that reported in the original work, where the reflectance phase shift was not measured. The M1 optical gap is nearly the same as that in the M2 and T phases, and similar optical interband features are present in all three phases.

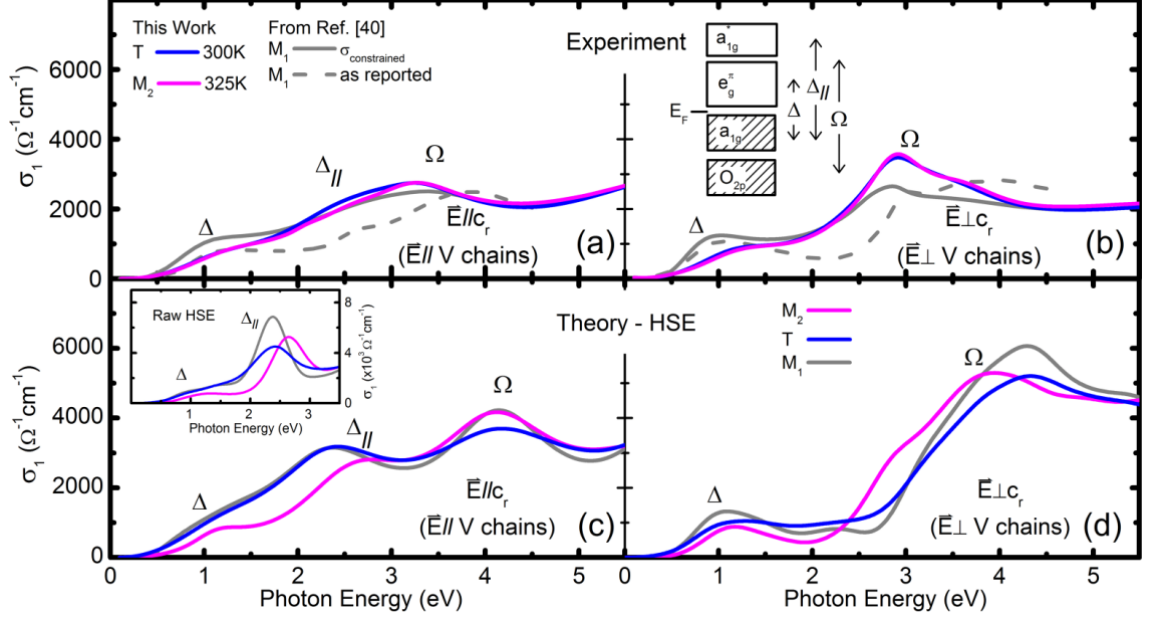


FIG. 3.2: Experimental optical conductivity σ_1 of the M2 and triclinic T phases parallel to the vanadium (V) chains (a) and perpendicular to the vanadium (V) chains (b). Phonon features, which occur below 0.11 eV, are not shown. For comparison, accurate optical conductivity of the M1 phase is extracted from the reflectance spectrum reported in [75] by using the complex conductivity of the T phase measured in this work as a constraint above 4 eV (see text). The inset in panel (b) shows an effective energy level diagram along with optical interband transitions that appear in the conductivity spectra. First-principles DFT optical conductivities calculated via the HSE functional are presented in (c) and (d). The calculated “raw” conductivities are broadened by 0.3 eV. The calculated conductivity for $E_{\parallel c_r}$ contains a very sharp Δ_{\parallel} feature [see inset of panel (c)]. To account for lifetime effects not handled in the static HSE treatment, the Δ_{\parallel} feature, which is assigned to transitions between the lower and upper Hubbard bands in the Mott picture, is further broadened to a FWHM of 1.5 eV in the main panel of (c), which better models the experiment.

The results of our hybrid DFT calculations are presented in Figs.3.2(c) and 3.2(d). In agreement with experimental measurements, we find that the energy values of the interband transitions, particularly Δ across the optical gap, are quite similar for all three phases. DFT+ U calculations ($U = 5.7$ eV and $J = 0.8$ eV, using LDAUTYPE = 1 in VASP, not shown) yield qualitatively similar results. This insensitivity to the change in lattice structure in all three insulating phases is incompatible with the Peierls picture. It is interesting to note that the Δ_{\parallel} feature in the raw HSE result is much sharper than in experiment (see Fig. 4). This is indicative of short lifetimes for carriers excited between the bonding and antibonding a_{1g} bands in the real system that is not captured in the static HSE theory. Such lifetime broadening is characteristic of significant electron-electron interactions in these orbitals of Mott-Hubbard character. This is additional evidence that the splitting of the a_{1g} bands, and consequently the energy gap, arises from Coulomb correlations. The most recent iteration of dynamical mean-field theory electronic structure calculations finds energy gaps for the M1 and M2 phases that are consistent with our experimental results [38].

A schematic of the effective electronic structure of the vanadium d bands for the three insulating VO₂ phases is shown in the inset of Fig. 3.2(b). There are two features of particular note, labeled Δ and Δ_{\parallel} . The interband transition Δ across the energy gap is centered about 1.2 eV for all three phases and has little polarization dependence. Similarly, Δ_{\parallel} occurs around 2.5 eV in all phases for light polarized along the vanadium chains, and is thus ascribed to transitions between the bonding and antibonding a_{1g} bands. These can

be thought of as the lower and upper Hubbard bands in the Mott picture. The features labeled Ω occur at 3 eV or higher energies and are primarily optical interband transitions between O_{2p} states and the empty vanadium d states. We emphasize that the robustness of the insulating phase band structure, despite the change in lattice structure, is a remarkable result that is not anticipated by conventional band theory.

3.5 Conclusions

To conclude, the nature of the VO_2 insulating phases is now clear. The optical spectroscopy data and the computational result presented here clearly demonstrates that the electronic structure of the VO_2 insulating phases is robust to changes in lattice structure and vanadium-vanadium pairing. In particular, the energy gap is insensitive to the dimerization of the equally spaced vanadium ions with localized electrons in the M2 chains. This result is incompatible with a Peierls gap and is strong evidence that the gap arises due to Mott-Hubbard type Coulomb correlations. The negative Knight shift is indicative of localized electrons on the equally spaced vanadium ions in the M2 chains. Its absence in the dimerized chains of all three phases [18] elucidates the key subtlety of the insulating VO_2 states: in contrast to a more conventional Mott insulator, where valence electrons are localized on individual ions, the dimerized vanadium chains contain bonded spin singlets which are localized on the vanadium dimers. This fact has made it difficult to conclusively distinguish between the Peierls and Mott-Hubbard pictures in the exhaustively studied M1 phase. Study of the M2 and T phases, with their nonequal V chains, is essential to

decouple the effects of dimerization and electronic correlations. Seen in a broader context, our work paves a path for disentangling the contributions of the electronic and structural degrees of freedom to phase transitions in other correlated electron systems.

CHAPTER 4

DFT+ U and HSE Investigation of the VO₂ Insulator-Metal Transition Under High Pressures

As mentioned, VO₂ is a transition metal oxide that exhibits a metal-insulator transition upon cooling below its critical temperature $T_c \approx 340$ K. This transition is accompanied by a simultaneous structural phase transition (SPT) from a tetragonal rutile R to a monoclinic M1 structure. Other insulating phases, another monoclinic M2 phase and a triclinic T, have been identified and are accessible via tensile strain[14] or chemical doping[16]. In addition to the SPT, electron-electron interaction effects also play an important role. For example, regular density functional theory (DFT) band structures predict metallic behavior or show only a small energy gap[31] in the monoclinic phases.

Recent work has focused on unraveling the relative importance of these two effects. It has been pointed out[10] that one way to accomplish this decoupling is by examining the other insulating phases, especially M2, as we recently did[76]. While most previous work has focused on the temperature-induced MIT, metallization has also been observed to occur on monoclinic VO₂ samples under sufficiently high pressures. In this chapter, we focus on this pressure-induced MIT.

Although explicit many-body calculations for this problem are still beyond the practical limits of current technology, advances in computing have made practical ever more sophisticated computational methods and techniques. In recent years several studies have successfully used dynamical mean-field theory (DMFT)[37, 38] [[and quantum Monte Carlo (QMC)[45] techniques]] to describe different aspects of VO₂. It was found that while a single-site impurity model is sufficient to describe the rutile R phase, the same model predicts a metallic M1 phase; a cluster-DMFT treatment where the M1 vanadium dimer is considered as a two-site impurity model is then required to open the insulating gap. While this underscores the entanglement of structural and electron-electron interaction effects, it also highlights the drawback of this approach, namely the choice of impurity models to properly describe each phase.

The simultaneity of the MIT and the SPT in the M1→R transition has been a source of no small confusion because it blurs the lines between cause and effect. In our previous work we decoupled these two aspects by calculating the optical conductivities of the three insulating phases via DFT+*U* and hybrid-DFT, specifically the Heyd-Scuseria-Ernzerhof

(HSE) functional. Both methods attempt to account for localized electron-electron interaction beyond what is accounted for in standard DFT. We found that the HSE results were in remarkable agreement with experiment, much more than the DFT+ U calculations. Moreover, we found the optical gap to be insensitive to the structural differences between the three insulating phases, and this was the case in both computed and measured optical data. From the experimental observations and our calculations[76], it can be concluded that intra-atomic Coulomb correlation, and not the structural change due to vanadium-vanadium pairing, is mainly responsible for the optical energy gap in the insulating phases of VO₂.

Previously in 2007 Arcangeletti *et al.*[18] reported a so-called isostructural transition from the insulating M1 phase into a metallic monoclinic phase under sufficiently high pressures. More recently, Bai *et al.*[19] reported that VO₂ in both M1 and R phases would transition into a metallic phase X above $P_c^{M1} = 34.3$ GPa and $P_c^R = 38.3$ GPa, respectively. Although its crystal structure could not be definitively identified, the structure of X was successfully indexed with a baddeleyite-like monoclinic unit cell ($P2_1/c$ symmetry). Another recent work by Lee *et al.*[77] describes a similar isostructural transition in thin-film VO₂. The existence of this high-pressure phase thus provides another pathway to decouple the electronic and structural aspects of the VO₂ metal-insulator transition.

Following the experimental work on phase X, He *et al.*[39] performed DFT+ U calculations on the M1 phase under increasing pressure. They identified two nearly-degenerate monoclinic phases (dubbed M1' and M1'') above 20 GPa whose structures are primarily

distinguished by opposite rotations of their oxygen octahedra with respect to the ambient-pressure M1 structure. Under increasing pressure, it was found that the M1'' energy gap would go to zero at 40 GPa, while M1' would maintain a sizeable insulating gap. Notably, this pressure-induced MIT in M1'' is not accompanied by a structural transition, as both phases retain their monoclinic symmetry. M1'' was therefore suggested as a possible explanation for the previously observed metallization of monoclinic VO₂ under high pressures.

In this chapter, we re-examine this finding, applying DFT+ U and HSE to study the pressure-induced MIT. After a brief description of the methodology, we will present our results and discuss the sensitivity of the calculations to the choice of DFT+ U formulation and compare these to HSE results. Both DFT+ U formulations fail to find reasonable metallization pressures, while our HSE calculations predict that the M1'' phase becomes metallic at ~ 32 GPa, in good agreement with the measured experimental value of 34.3 GPa.

4.1 Computational Methods

As in the previous chapter, we account for the strong correlation of the d -electrons using DFT+ U calculations utilizing either the Liechtenstein[24] or Dudarev[25] approach to model the Hubbard interaction. The former treats the on-site Coulomb parameter U and exchange parameter J as independent correction terms, while the latter is a simplified approach in which only a single effective parameter $U_{\text{eff}} = U - J$ accounts for the Coulomb interactions.

It has been shown[28] that with a suitable choice of α , the HSE functional can provide a good description of electronic properties for the material being investigated. Moreover, the percentage of HSE exact exchange as represented by α can be linked to the Hubbard U in DFT+ U , and increasing values of α and U yield larger bandgaps[30]. That said, it should be noted that unlike the Hubbard U in DFT+ U which is applied only to the vanadium d -electrons, the HSE exact exchange α acts on all bands. In this sense HSE can be argued to be a less-parametrized approach to include strong correlation effects compared to DFT+ U .

For the hybrid-DFT calculations, a full relaxation from the experimental structure would have been expensive in terms of computation time. Therefore we made use of the relaxed DFT+ U structures as a starting point for our hybrid-DFT calculations: starting with the ambient M1 structure, we simulated an increase in external pressure P and fixed atomic positions while allowing the unit cell volume and shape to relax until there is no appreciable change ($\lesssim 0.1\%$ change in cell volume). The cell volume and shape are then fixed and the atomic positions are allowed to relax until residual forces were acceptably small ($\lesssim 0.01$ eV/Å). The process is repeated until sufficient convergence is reached, and the resulting structure is then used as a starting point for further relaxation using hybrid-DFT.

All *ab-initio* calculations were performed using the Vienna *Ab-initio* Simulations Package (VASP). DFT+ U calculations were completed using the Perdew-Burke-Ernzerhof (PBE) functional as implemented in VASP, and the values $U = 3.45$ eV and $J = 0.8$ eV ($U_{\text{eff}} = U - J = 2.65$ eV, using the Dudarev approach as implemented in VASP, LDAUTYPE =

2, unless otherwise specified) were used for the Hubbard parameter U and exchange parameter J . Hybrid-DFT calculations were performed using the HSE functional as implemented in VASP, with the choice of (screened) exact-exchange fraction $\alpha = 0.05$ and screening parameter $\mu = 0.2$. All calculations utilized an $8 \times 8 \times 8$ Monkhorst-Pack grid to sample the Brillouin zone.

4.2 Results and Discussion

Under increasing pressure, the oxygen octahedra of the insulating M1 phase simultaneously undergoes a compressive deformation and a near-rigid rotation about the rutile c_R axis. Both DFT+ U and hybrid-DFT calculations found two nearly-degenerate insulating phases M1' and M1'' above 20 GPa, structurally differentiated mainly by the sense of rotation of their oxygen octahedra under increasing pressures, in agreement with previous findings[39].

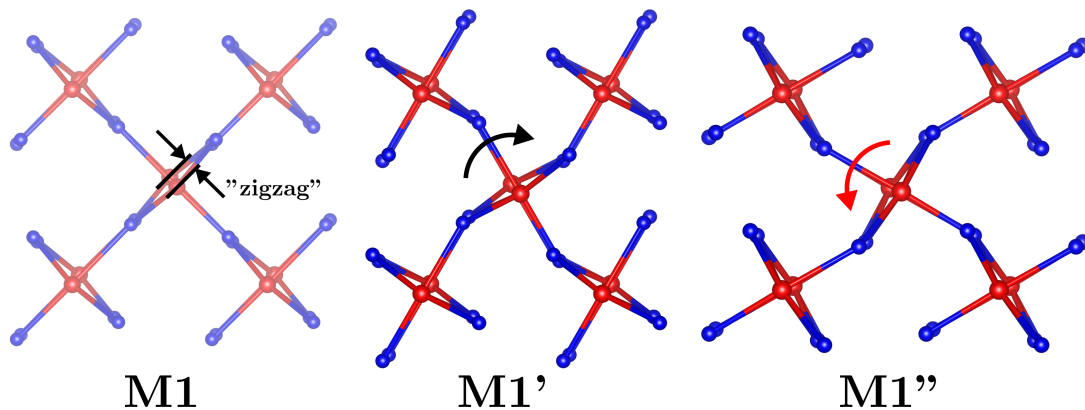


FIG. 4.1: M1 VO₂ at ambient pressure; M1' and M1'' at 100 GPa to emphasize the octahedral rotations, seen along the rutile c_R (monoclinic a_{M1}) direction. Vanadium atoms are red; oxygen atoms are a smaller blue. Zigzag distance is then defined as the distance between dimer V atoms when projected onto the rutile (001) (monoclinic (100)) plane.

Other than the oxygen octahedra rotations, the main structural features of the insulating M1 phase are the dimerization of the vanadium atoms and their tilting away from the rutile c_R direction; the latter is represented here by the "zigzag" distance as defined in Fig.4.1 above. However, apart from the opposite rotations of corresponding oxygen octahedra, we find that our DFT+ U calculation yielded little to no significant structural difference between M1' and M1'' even up to 100 GPa, as shown in Fig.4.2; specifically, no significant difference in cell volume, or short and long dimer bond lengths between the two phases were found.

Our Dudarev DFT+ U calculations failed to observe metallization of the M1'' structure throughout the entire pressure range, in disagreement with the previous report[39]. However, we do find a pronounced difference between M1' and M1'' in the response of the bandgap to the external pressure: while no metallization was observed, the bandgap of the M1'' phase was much more sensitive to external pressure, approaching ~ 0.1 eV at 100 GPa while M1' maintained a band gap of ~ 0.4 eV at the same pressure. Although broadening of the energy bands due to external pressure can partially explain the closing of the gap in both phases, it does not explain the difference of gap widths between them, from ~ 0.1 eV at 40 GPa to almost 0.3 eV at 100 GPa.

Our calculations using Liechtenstein[24] DFT+ U as implemented in VASP (LDAUTYPE = 1), with $U = 3.7$ eV and $J = 0.8$ eV¹ results in a similar outcome: a pronounced difference between M1' and M1'' in the bandgap as a function of external pressure despite little to no structural differentiation, with the exception that M1'' was found to become metallic

¹These values were chosen to match the HSE gap at $\alpha = 0.05$.

at 100 GPa.

The hybrid-DFT HSE calculations again find little structural differentiation between M1' and M1"; the bandgap response however, is now markedly different. We find that HSE predicts that M1" becomes metallic at ~ 32 GPa, in good agreement with experimental measurements[19]. Interestingly, this transition pressure seems to not be sensitive to the specific details of the structural relaxation, with a similar transition pressure found with hybrid-DFT calculations done with structures obtained by relaxation via DFT+ U .

Using WANNIER90 and Wannier function k-point interpolation we generate maximally-localized Wannier functions (MLWFs) to visualize the band structures of the M1' and M1" phases. Partial-DOS calculations were done to determine orbital characters of the bands. At 30 GPa, just below the critical pressure, we find both phases to be insulating; moreover, their bands retain the orbital characteristics of the M1 phase as described by Goodenough[20], as shown in Fig.4.4. Thus aside from the smaller gap in M1", we find no qualitative difference between the electronic band structures of the two phases in the insulating state at this pressure.

At 100 GPa the M1" phase is fully metallic, with a ~ 0.5 eV overlap between the bonding a_{1g} and the e_g^π bands. M1' remains insulating albeit with a greatly diminished energy gap of ~ 0.1 eV. Meanwhile, in both phases the high pressure has lifted the antibonding a_{1g}^* bands above the e_g^π manifold to be easily distinguishable. Visualization of the generated MLWFs once again confirm the orbital assignments, but fails to provide any further hints on the origin of the discrepancy.S

4.3 Conclusions

DFT+ U and hybrid-DFT calculations were performed on the insulating M1 phase of VO₂ under increasingly higher pressure. Above 20 GPa both methods find two nearly-degenerate phases M1' and M1'' that are structurally differentiated mainly by opposite rotations of their oxygen octahedra about the rutile c_R axis. Both DFT+ U and hybrid-DFT find little to no difference in the cell volumes, V-V bond lengths, or dimer tilts between these high-pressure phases. Despite this structural similarity the energy gap response to pressure between the two phases is markedly different, with M1'' tending toward metallization at a much more rapid rate than M1'. Critically, where DFT+ U fails to find a reasonable metallization pressure, hybrid-DFT HSE calculations predict that the M1'' phase becomes metallic at ~ 32 GPa, in good agreement with experimental measurements of a metallic monoclinic state at 34.3 GPa. Although much more work needs to be done to determine the origin of this metallization, these results reinforce our previous finding[76] that electronic correlation, and not structural distortion, is the primary mechanism behind the energy gap in insulating VO₂. Moreover, HSE appears to capture this correlation in a manner superior to DFT+ U , though the specifics of how this is achieved remain to be fully described.

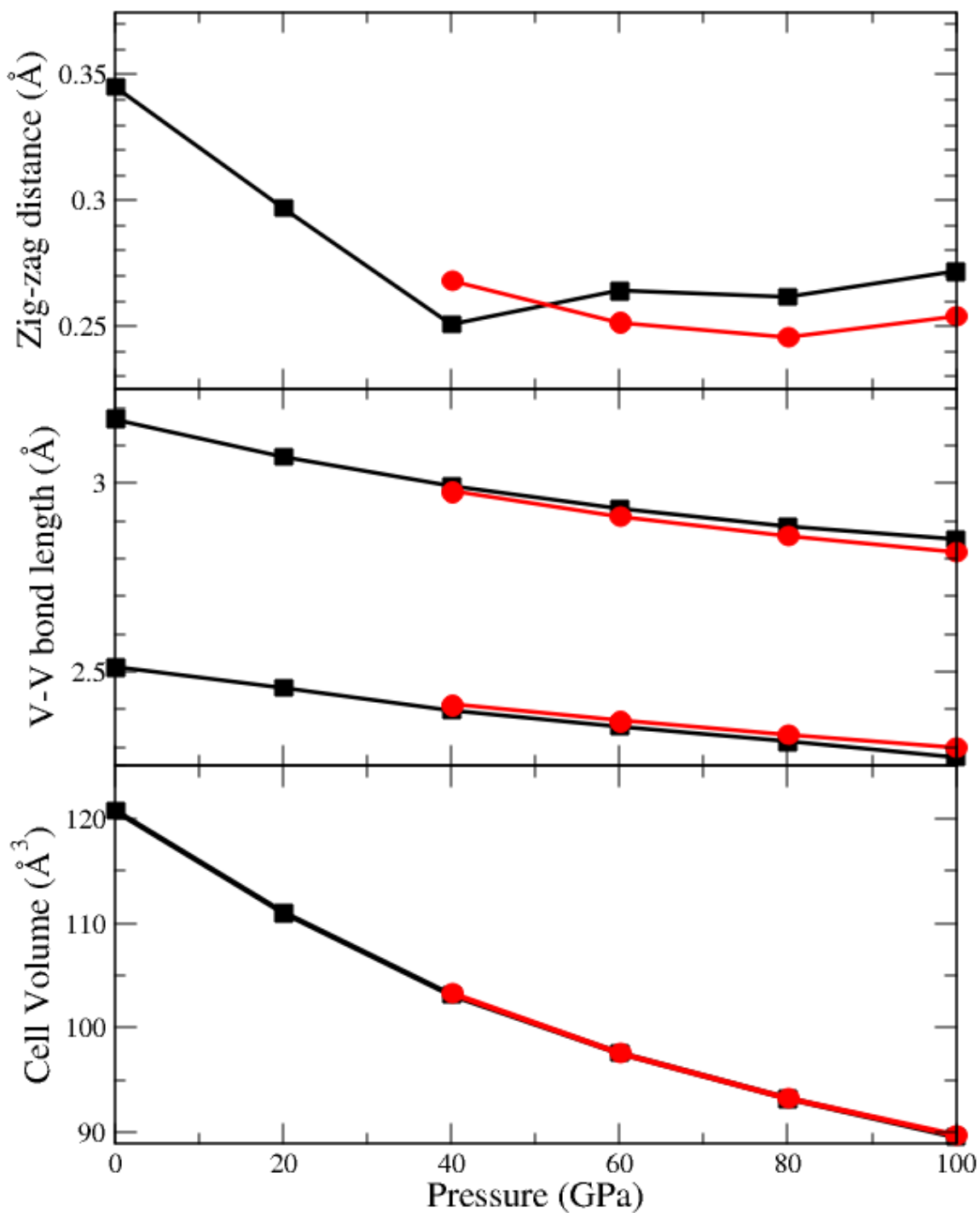


FIG. 4.2: Comparison of structural properties in M1' and M1'' as calculated via DFT+ U ; from top to bottom: (a) zig-zag distance, (b) V-V bond lengths, and (c) cell volumes. Black lines with square symbols denote M1'; red lines with circle symbols, M1''.

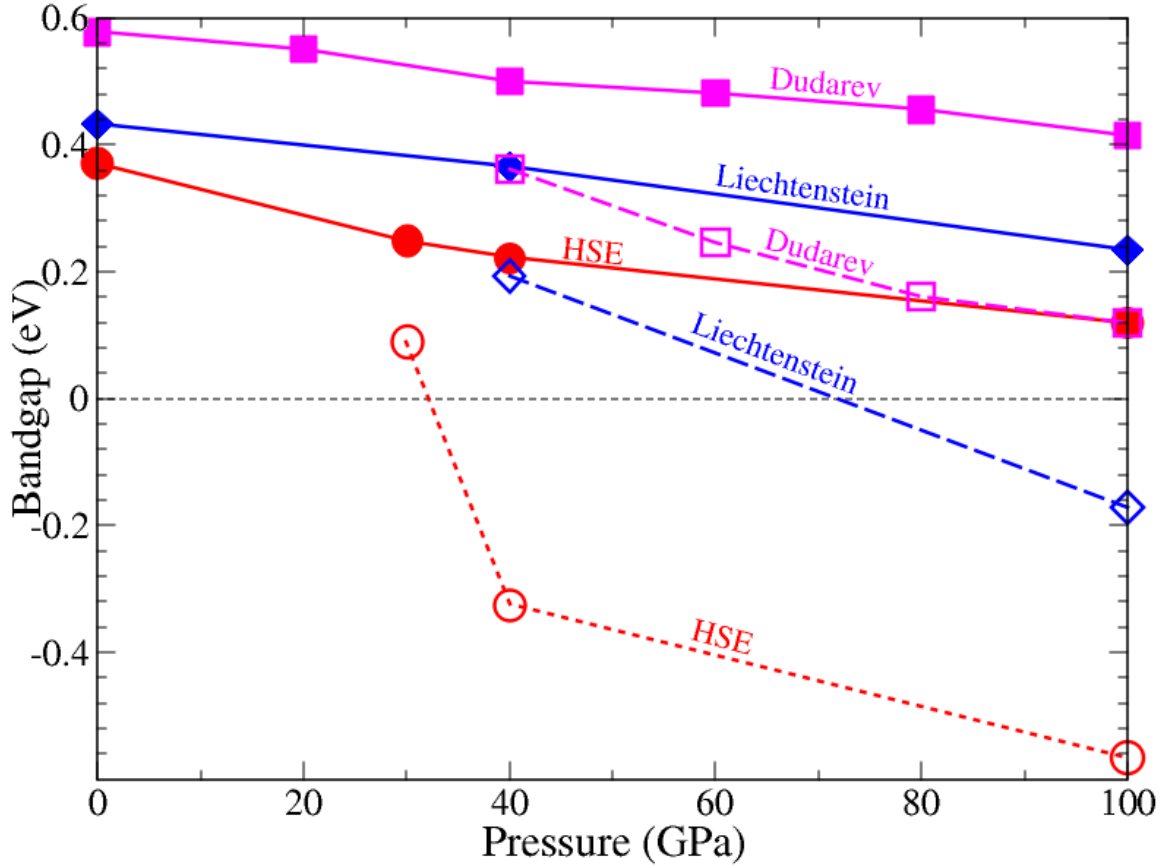


FIG. 4.3: Bandgap as a function of external pressure as calculated using DFT+ U and HSE as implemented in VASP. Negative values indicate an overlap of the a_{1g} and e_g^π bands instead of a gap, as shown in Fig.4.5. Circles, diamonds and squares denote HSE, Liechtenstein DFT+ U and Dudarev DFT+ U , respectively. Solid lines denote M1'; dashed lines denote M1''. Note that the Liechtenstein calculations predict a metallic M1'', but at a much higher pressure compared to HSE. In contrast to a previous study[39] which finds metallization of M1'' at 40 GPa, our Dudarev calculations fail to find any metallization whatsoever over the entire pressure range.

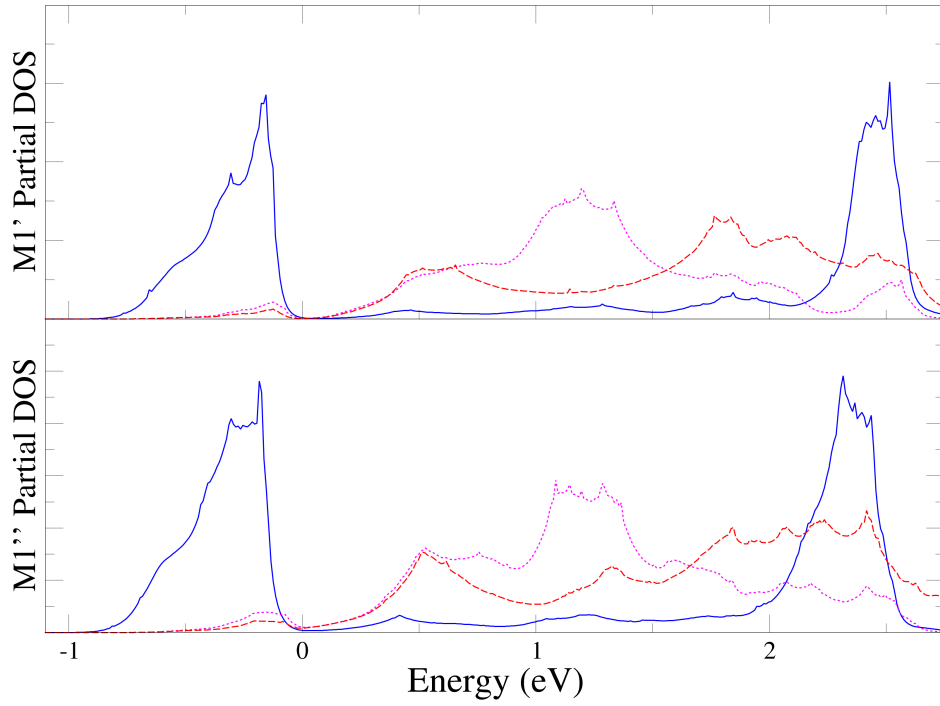


FIG. 4.4: Partial DOS of select vanadium orbitals for M1' (top) and M1''(bottom) at 30 GPa generated using WANNIER90. Solid blue lines indicate $d_{x^2-y^2}$ orbital character, dashed red lines indicate d_{yz} , and dotted magenta lines indicate d_{xz} . The band gap appears smaller than reported due to adaptive smearing employed by WANNIER90 in the process of generating DOS plots.

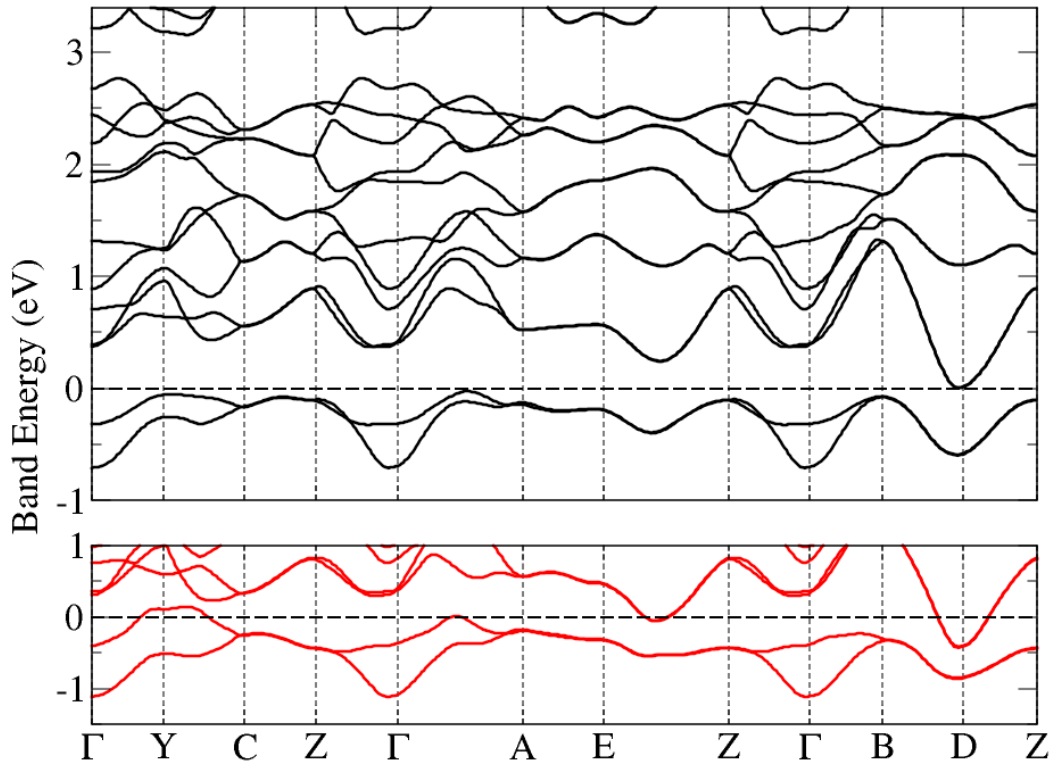


FIG. 4.5: Band structure of M1'' at 30 GPa(top) and 100 GPa(bottom) as calculated using HSE and visualized via WANNIER90. At 30 GPa M1'' is still a small-gap (~ 0.1 eV) insulator, while at 100 GPa there is a large overlap (~ 0.5 eV) of the a_{1g} and e_g^π manifolds.

CHAPTER 5

Conclusions and Outlook

At this point it is clear that the insulating gap of VO_2 is driven mainly by strong correlation effects. The lack of appreciable changes in the band structure throughout the $\text{M2} \rightarrow \text{T} \rightarrow \text{M1}$ transition is incompatible with the idea that the insulating gap is dominated by structural effects such as in the case of Peierls transitions. Moreover, our work on the high-pressure phases $\text{M1}'$ and $\text{M1}''$ clearly show that structural parameters such as dimer length, which are of prime importance in the classic Peierls-like mechanism, appear to be poorly correlated to overall electronic structure. We are thus left with the conclusion that VO_2 must be a Mott insulator.

Having said that, settling the question of the mechanism of the insulating gap is just one step toward full characterization of VO_2 . As the results of our high-pressure calculations on VO_2 demonstrate, there appears to be some subtle interplay between the lattice structure and electronic correlations that is not yet understood. Further study of

the metallic monoclinic phase, via experimental measurements and computational models, will be needed to gain deeper insight into the workings of this subtle interplay.

Finally, our work shows that there remains a place for DFT in the study of correlated materials such as VO_2 . Despite not being as sophisticated as more recent methods such as DMFT, our work indicates that with some further refinement, hybrid-DFT methods such as HSE- α may possess predictive power that can greatly assist experimental characterization of correlated systems such as VO_2 . If realized, this would be an important step toward harnessing VO_2 in real-world device applications.

BIBLIOGRAPHY

- [1] H. Bethe, *Ann. Phys. (Leipzig)* **87**, 55 (1928).
- [2] A. Sommerfeld, *Z. Phys.* **47**, 1 (1929).
- [3] F. Bloch, *Z. Phys.* **57**, 545 (1929).
- [4] R. Peierls, *Proc. Phys. Soc. London, Ser. A* **49**, 72 (1929).
- [5] N. F. Mott, *Proc. Phys. Soc. London, Ser. A* **49**, 72 (1929).
- [6] N. F. Mott, *Proc. Phys. Soc. London, Ser. A* **62**, 416 (1949).
- [7] N. F. Mott, *Can. J. Phys.* **34**, 1356 (1956).
- [8] N. F. Mott, *Philos. Mag.* **6**, 287 (1961).
- [9] F. J. Morin, *Phys. Rev. Lett.* **3**, 34 (1959).
- [10] J. P. Pouget, H. Launois, T. M. Rice, P. Dernier, A. Gossard, G. Villeneuve, and P. Hagemuller, *Phys. Rev. B* **10**, 1801 (1974).
- [11] P. Hohenberg and W. Kohn, *Phys. Rev.* **136** (1964).
- [12] W. Kohn and L. J. Sham, *Phys. Rev.* **140**, A1133 (1965).
- [13] M. Imada, A. Fujimori, and Y. Tokura, *Rev. Mod. Phys.* **70**, 1039 (1998).
- [14] J. H. Park, J. M. Coy, T. S. Kasirga, C. Huang, Z. Fei, S. Hunter, and D. H. Cobden, *Nature* **500**, 431 (2013).

- [15] D. B. McWhan, M. Marezio, J. P. Remeika, and P. D. Dernier, *Phys. Rev. B* **10**, 490 (1974).
- [16] M. Marezio, D. B. McWhan, J. P. Remeika, and P. D. Dernier, *Phys. Rev. B* **5**, 2541 (1972).
- [17] G. Villeneuve, M. Drillon, and P. Hagemuller, *Mater. Res. Bull.* **8**, 1111 (1973).
- [18] E. Arcangeletti, L. Baldassarre, D. D. Castro, S. Lupi, L. Malavasi, C. Marini, A. Perucchi, and P. Postorino, *Phys. Rev. Lett.* **98**, 196406 (2007).
- [19] L. Bai, Q. Li, S. A. Corr, Y. Meng, C. Park, S. V. Sinogeikin, and C. Ko, *Phys. Rev. B* **91**, 104110 (2015).
- [20] J. B. Goodenough, *J. Solid State Chem.* **3**, 490 (1971).
- [21] J. M. Longo and P. Kierkegaard, *Acta Chem. Scand.* **24**, 420 (1970).
- [22] V. Eyert, *Ann. Phys. (Leipzig)* **11**, 9 (2002).
- [23] A. Zylbersztejn and N. F. Mott, *Phys. Rev. B* **11**, 4383 (1975).
- [24] A. I. Liechtenstein, V. I. Anisimov, and J. Zaanen, *Phys. Rev. B* **52**, R5467 (1995).
- [25] S. L. Dudarev, G. A. Botton, S. Y. Savrasov, C. J. Humphreys, and A. P. Sutton, *Phys. Rev. B* **57**, 1505 (1998).
- [26] O. Bengone, M. Alouani, P. Blöchl, and J. Hugel, *Phys. Rev. B* **62**, 16392 (2000).
- [27] A. Rohrbach, J. Hafner, and G. Kresse, *J. Phys.: Condens. Matter* **15**, 979–996 (2003).
- [28] J. He and C. Franchini, *Phys. Rev. B* **86**, 235117 (2012).

- [29] C. Franchini, *J. Phys.: Condens. Matter* **26**, 253202 (2014).
- [30] V. Ivády, R. Armiento, K. Szász, E. Janzén, A. Gali, and I. A. Abrikosov, *Phys. Rev. B* **90**, 035146 (2014).
- [31] R. M. Wentzcovitch, W. W. Schulz, and P. B. Allen, *Phys. Rev. Lett.* **72**, 3389 (1994).
- [32] T. M. Rice, H. Launois, and J. P. Pouget, *Phys. Rev. Lett.* **73**, 3042 (1994).
- [33] V. Eyert, *Phys. Rev. Lett.* **107**, 016401 (2011).
- [34] T. J. Huffman, P. Xu, M. M. Qazilbash, E. J. Walter, H. Krakauer, J. Wei, D. H. Cobden, H. A. Bechtel, M. C. Martin, G. L. Carr, et al., *Phys. Rev. B* **87**, 115121 (2013).
- [35] S. Biermann, A. Poteryaev, A. I. Lichtenstein, and A. Georges, *Phys. Rev. Lett.* **94**, 26404 (2005).
- [36] J. M. Tomczak and S. Biermann, *Phys. Rev. B.* **80**, 85117 (2009).
- [37] C. Weber, D. D. O'Regan, N. D. M. Hine, M. C. Payne, G. Kotliar, and P. B. Littlewood, *Phys. Rev. Lett.* **108**, 256402 (2012).
- [38] W. Brito, M. Aguiar, K. Haule, and G. Kotliar, *Phys. Rev. Lett.* **117**, 056402 (2016).
- [39] H. He, H. Gao, W. Wu, S. Cao, J. Hong, D. Yu, G. Deng, Y. Gao, P. Zhang, H. Luo, et al., *Phys. Rev. B* **94**, 205127 (2016).
- [40] A. Perucchi, L. Baldassarre, P. Postorino, and S. Lupi, *J. Phys. Condens. Matter* **21**, 323202 (2009).
- [41] D. N. Basov, R. D. Averitt, D. van der Marel, M. Dressel, and K. Haule, *Rev. Mod. Phys.* **83**, 471 (2011).

- [42] A. X. Gray, J. Jeong, N. P. Aetukuri, P. Granitzka, Z. Chen, R. Kukreja, D. Higley, T. Chase, A. H. Reid, H. Ohldag, et al., *Phys. Rev. Lett.* **116**, 116403 (2016).
- [43] J. D. Budai, J. Hong, M. E. Manley, E. D. Specht, C. W. Li, J. Z. Tischler, D. L. Abernathy, A. H. Said, B. M. Leu, L. A. Boatner, et al., *Nature (London)* **515**, 535 (2014).
- [44] M. Gatti, F. Sottile, and L. Reining, *Phys. Rev. B* **91**, 195137 (2015).
- [45] H. Zheng and L. K. Wagner, *Phys. Rev. Lett.* **114**, 176401 (2015).
- [46] T. C. Koethe, Z. Hu, M. W. Haverkort, C. Schußler-Langeheine, F. Venturini, N. B. Brookes, O. Tjernberg, W. Reichelt, H. H. Hsieh, H.-J. Lin, et al., *Phys. Rev. Lett.* **97**, 116402 (2006).
- [47] R. Eguchi, M. Taguchi, M. Matsunami, K. Horiba, K. Yamamoto, Y. Ishida, A. Chainani, Y. Takata, M. Yabashi, D. Miwa, et al., *Phys. Rev. B* **78**, 075115 (2008).
- [48] M. W. Haverkort, Z. Hu, A. Tanaka, W. Reichelt, S. V. Streltsov, M. A. Korotin, V. I. Anisimov, H. H. Hsieh, H. J. Lin, C. T. Chen, et al., *Phys. Rev. Lett.* **95**, 196404 (2005).
- [49] V. R. Morrison, R. P. Chatelain, K. L. Tiwari, A. Hendaoui, A. Bruhacs, M. Chaker, and B. J. Siwick, *Science* **346**, 445 (2014).
- [50] D. Wegkamp, M. Herzog, L. Xian, M. Gatti, P. Cudazzo, C. L. McGahan, R. E. Marvel, R. F. Haglund, A. Rubio, M. Wolf, et al., *Phys. Rev. Lett.* **113**, 216401 (2014).
- [51] B. T. O’Callahan, A. C. Jones, J. H. Park, D. H. Cobden, J. M. Atkin, and M. B. Raschke, *Nat. Commun.* **6**, 6849 (2015).

- [52] D. Wegkamp and J. Stahler, *Prog. Surf. Sci.* **90**, 464 (2015).
- [53] B. Mayer, C. Schmidt, A. Grupp, J. Buhler, J. Oelmann, R. E. Marvel, R. F. Haglund, T. Oka, D. Brida, A. Leitenstorfer, et al., *Phys. Rev. B* **91**, 235113 (2015).
- [54] K. Okazaki, S. Sugai, Y. Muraoka, and Z. Hiroi, *Phys. Rev. B* **73**, 165116 (2006).
- [55] M. M. Qazilbash, M. Brehm, B.-G. Chae, P.-C. Ho, G. O. Andreev, B.-J. Kim, S. J. Yun, A. V. Balatsky, M. B. Maple, F. Keilmann, et al., *Science* **318**, 1750 (2007).
- [56] M. M. Qazilbash, A. A. Schafgans, K. S. Burch, S. J. Yun, B. G. Chae, B. J. Kim, H. T. Kim, and D. N. Basov, *Phys. Rev. B* **77**, 115121 (2008).
- [57] T. J. Huffman, P. Xu, A. J. Hollingshad, M. M. Qazilbash, L. Wang, R. A. Lukaszew, S. Kittiwatanakul, J. Lu, and S. A. Wolf, *Phys. Rev. B* **91**, 205140 (2015).
- [58] M. Nazari, Y. Zhao, V. V. Kuryatkov, Z. Y. Fan, A. A. Bernussi, and M. Holtz, *Phys. Rev. B* **87**, 035142 (2013).
- [59] M. Ghedira, J. Chenavas, and M. Marezio, *J. Phys. C* **10**, L309 (1977).
- [60] T. Kong, M. W. Masters, S. L. Bud'ko, and P. C. Canfield, *APL Mater.* **3**, 041502 (2015).
- [61] E. Strelcov, A. Tselev, I. Ivanov, J. D. Budai, J. Zhang, J. Z. Tischler, I. Kravchenko, S. V. Kalinin, and A. Kolmakov, *Nano Lett.* **12**, 6198 (2012).
- [62] J. P. Pouget, H. Launois, J. P. Dhaenens, P. Merenda, and T. M. Rice, *Phys. Rev. Lett.* **35**, 873 (1975).
- [63] J. P. Dhaenens, D. Kaplan, and P. Merenda, *J. Phys. C* **8**, 2267 (1975).

- [64] B. S. Mun, K. Chen, Y. Leem, C. Dejoie, N. Tamura, M. Kunz, Z. Liu, M. E. Grass, C. Park, J. Yoon, et al., *Phys. Status Solidi RRL* **5**, 107 (2011).
- [65] B. S. Mun, K. Chen, J. Yoon, C. Dejoie, N. Tamura, M. Kunz, Z. Liu, M. E. Grass, S.-K. Mo, C. Park, et al., *Phys. Rev. B* **84**, 113109 (2011).
- [66] M. Ghedira, H. Vincent, M. Marezio, and J. C. Launay, *J. Solid State Chem.* **22**, 423 (1977).
- [67] J. Heyd, G. E. Scuseria, and M. Ernzerhof, *J. Chem. Phys.* **118**, 8207 (2003).
- [68] J. Heyd, G. E. Scuseria, and M. Ernzerhof, *J. Chem. Phys.* **124**, 219906 (2006).
- [69] M. Gajdoš, K. Hummer, G. Kresse, J. Furthmüller, and F. Bechstedt, *Phys. Rev. B* **73**, 045112 (2006).
- [70] G. Kresse and J. Hafner, *Phys. Rev. B* **47**, 558–561 (1993).
- [71] G. Kresse and J. Furthmüller, *Phys. Rev. B* **54**, 11169 (1996).
- [72] G. Kresse and J. Furthmüller, *Comput. Mater. Sci.* **6**, 15–50 (1996).
- [73] G. Kresse and D. Joubert, *Phys. Rev. B* **59**, 1758–1775 (1999).
- [74] N. F. Quackenbush, H. Paik, M. J. Wahila, S. Sallis, M. E. Holtz, X. Huang, A. Ganose, B. J. Morgan, D. O. Scanlon, Y. Gu, et al., *Phys. Rev. B* **94**, 085105 (2016).
- [75] H. W. Verleur, A. S. Barker, and C. N. Berglund, *Phys. Rev.* **172**, 788 (1968).
- [76] T. Huffman, C. Hendriks, E. J. Walter, J. Yoon, H. Ju, R. Smith, G. L. Carr, H. Krakauer, and M. M. Qazilbash, *Phys. Rev. B* **95**, 075125 (2017).

- [77] D. Lee, B. Chung, Y. Shi, G.-Y. Kim, N. Campbell, F. Xue, K. Song, S.-Y. Choi, J. P. Podkaminer, T. H. Kim, et al., *Science* **362**, 1037 (2018).

VITA

Christopher Hendriks

Christopher was born in Ambon, Indonesia. He attended Universitas Pelita Harapan in Indonesia and graduated in 2007 with an S.Si in physics. In 2011 he began his doctoral studies at the College of William and Mary, where he later joined Henry Krakauer's research group and studied the nature of the metal-insulator transition in vanadium dioxide via density functional theory.